Simulation model of concentrated colloidal nanoparticulate flows

Masahiro Fujita and Yukio Yamaguchi
Department of Chemical System Engineering, The University of Tokyo, Bunkyo-ku, Tokyo 113-8656, Japan
(Received 13 June 2007; published 25 February 2008)

This paper presents a simulation model of concentrated colloidal nanoparticulate flows to investigate self-organization of the nanoparticles and rheology of the colloid. The motion of solid nanoparticles is treated by an off-lattice Newtonian dynamics. The flow of solvent is treated by an on-lattice fluctuating Navier-Stokes equation. A fictitious domain method is employed to couple the motion of nanoparticles with the flow of solvent. The surface of nanoparticles is expressed by discontinuous solid-liquid boundary to calculate accurately contact interaction and Derjaguin-Landau-Verwey-Overbeek interaction between the nanoparticles. At the same time, the surface is expressed by continuous solid-liquid boundary to calculate efficiently hydrodynamic interaction between the nanoparticles and the solvent. Unlike other simulation models that focus on the hydrodynamic interaction, the present model includes all crucial interactions, such as contact force and torque, van der Waals force, electrostatic force, hydrodynamic force, and torque including thermal fluctuation of the solvent that causes translational and rotational Brownian motions of the nanoparticles. Especially the present model contains the frictional force that plays a significant role on nanoparticles in contact with one another. A fascinating novelty of the present model is that computational cost is constant regardless of the concentration of nanoparticles. The capability of the present simulation model is demonstrated by two-dimensional simulations of concentrated colloidal nanoparticles in simple shear flows between flat plates. The self-organization of concentrated colloidal nanoparticles and the viscosity of colloid are investigated in a wide range of Péclet numbers.

DOI: 10.1103/PhysRevE.77.026706 PACS number(s): 47.11.−j, 47.57.−s, 47.61.−k, 05.65.+b

I. INTRODUCTION

Recently, self-organization of colloidal nanoparticles is gathering a lot of attention in the field of materials nanotechnology. Typical nanoscale structures, such as crystals, thin films and composites that contain metal, semiconductor, or polymer nanoparticles, are often made by coating-drying processes of colloids [1–8]. In the processes, concentrated colloidal nanoparticles have an autonomous structure formation in a flow that is called self-organization. It is important to elucidate mechanism of the self-organization to control the structure of nanoparticles. The self-organization of concentrated colloidal nanoparticles is caused by various interactions between nanoparticles and between nanoparticles and a solvent, such as contact interaction, DLVO (Derjaguin-Landau-Verwey-Overbeek) interaction, hydrodynamic interaction including thermal fluctuation of the solvent. The interactions have mesoscopic scales that lie between microscopic molecular scale and macroscopic continuum scale. Simulation of the colloidal nanoparticulate flows is a major challenge even now when computational fluid dynamics is well developed, because typical simulation methods are based on either the microscopic or macroscopic single-phase model. Especially, concentrated systems are difficult to solve since the interactions are strongly coupled with one another.

A significant number of authors have ever addressed mesoscopic solid-liquid two-phase modeling. Main issues on the modeling are the treatment of hydrodynamic interaction that satisfies the fluctuation-dissipation theorem and the treatment of moving solid-liquid boundaries. Existing simulation models are categorized by the treatment of liquid into the off-lattice model and the off-lattice–on-lattice hybrid model. Brownian-Stokesian dynamics (BSD) [9–13] is a well-developed off-lattice model. The model treats the motion of particles that have discontinuous solid-liquid boundaries by the Langevin equation without treatment of the liquid flow. The hydrodynamic interaction is introduced through configuration-dependent resistance tensors into a resistive term and a stochastic term of the Langevin equation. Although it is not necessary to solve the flow of liquid, the computational effort to obtain the resistance tensors at each time step is rather expensive in the case of a concentrated system. The model has been applied to extremely low Reynolds number flows where the approximation of Stokes flow is valid. Dissipative particle dynamics (DPD) [14–17] is a rapidly spreading off-lattice model. The model treats liquid as an ensemble of dissipative particles that exchange momenta with one another in the stochastic manner and propagate based on the Newtonian dynamics. A solid particle can be expressed by an ensemble of dissipative particles that are fixed on the surface of solid particles. Therefore a solid particle has continuous solid-liquid boundary. The hydrodynamic interaction is automatically introduced through the momenta exchange between the fixed dissipative particles and surrounding free dissipative particles. A drawback of the model is that solid particles in contact are easily overlapped due to soft repulsive potential of the fixed dissipative particles.

The majority of mesoscopic solid-liquid two-phase models ever proposed are the off-lattice–on-lattice hybrid model. The hybrid model treats the motion of particles by the Newtonian dynamics, whereas the flow of liquid on a lattice is treated by a hydrodynamic equation. A possible hydrodynamic equation is the fluctuating Navier-Stokes equation [18–20]. The fluctuating Navier-Stokes equation is proposed by Landau and Lifshitz [18] at first, and is theoretically verified by Fox and Uhlenbeck [19]. The equation can naturally

reproduce the many-body Brownian motion of the particles that satisfies the fluctuation-dissipation theorem. Sharma and Patankar [21] and Atzberger [22] have computed the Brownian motion of particles in a liquid by use of off-lattice–on-lattice hybrid models that consist of the fluctuating Navier-Stokes equation and the immersed boundary (IB) method [23–25]. The IB method introduces a forcing term into a hydrodynamic equation to satisfy the no-slip condition on the surface of particles. A summation of every forcing term on a particle accelerates the particle. The propagation of particle obeys the Newtonian dynamics. The no-slip condition on the surface of particle is satisfied through an interpolation of velocity on the lattice points that do not coincide with the surface of particles. Therefore a particle has continuous solid-liquid boundary. The IB method consists of an explicit coupling of the hydrodynamic equation of liquid and the Newtonian dynamics of particles. In contrast, the distributed Lagrange multiplier with fictitious domain (DLMFD) method [26–28] consists of an implicit coupling of both equations. In the model, the solid particles are given as fictitious domains with the rigidity constraint. The combined equation that describes the motion of both solid and liquid is solved in the entire computational domain. The motion of particles and the flow of liquid evolve with a common time step. The DLMFD method and the IB method can be said to be the different numerical implementations of an essentially identical model. In the DLMFD method, the condition of rigid particle is forced in the particle domain, whereas the condition is forced on the surface of particle in the IB method. Yu [28] has computed Brownian particulate flows by use of an off-lattice–on-lattice hybrid model that consists of the nonfluctuating Navier-Stokes equation and the DLMFD method with a simplified Brownian random force. On the other hand, Tanaka and Araki [29] have developed an off-lattice–on-lattice hybrid model based on the fluctuating Stokes equation that is called fluid particle dynamics (FPD). The model treats a solid particle as a liquid of high viscosity, in which the binary fluctuating Stokes equation is solved on a lattice. The velocity of the particle is obtained from an arithmetic average of liquid velocities in the particle domain. The model represents a particle surface as a continuous variation of the particle density. A common time step is used for the motion of particles and the flow of liquid as the DLMFD method.

An alternative hydrodynamic equation on a lattice is the fluctuating lattice Boltzmann equation [30–36]. It is the lattice Boltzmann equation [37,38]. with a stochastic term representing thermal fluctuation. The equation can reproduce the many-body Brownian motion of the particles that satisfies the fluctuation-dissipation theorem as the fluctuating Navier-Stokes equation. Ladd [30–32] and Segrè [34] have computed Brownian motion of particles in a liquid by use of off-lattice–on-lattice hybrid models that consist of the fluctuating lattice Boltzmann equation and the Newtonian dynamics. They impose a no-slip boundary condition on intersections of the particle surface with the lattice. In a word, a particle is given as a polygon that has discontinuous solid-liquid boundary. Another hydrodynamic model has been suggested by Malevanets and Kapral [39,40] that is called stochastic rotation dynamics (SRD). The model treats liquid as an ensemble of particles that obey the Newtonian dynamics. The momenta of a liquid is transported by the stochastic collision of the liquid particles in a control volume on a lattice. The thermal fluctuation of liquid is naturally reproduced through the stochastic collision. The model can be said to be an intermediate between DPD and the direct simulation Monte Carlo (DSMC) method [41]. Hecht [42] and Padding [43] have computed Brownian motion of colloidal nanoparticles by use of off-lattice–on-lattice hybrid models that consist of the SRD and the Newtonian dynamics. In their simulations, the solid-liquid boundary is not treated explicitly, whereas simple repulsive potential is embedded between a liquid particle and a solid particle to describe the solid-liquid interaction.

Every model described above has enough capability to deal with the hydrodynamic interaction between dispersed solid particles and a liquid. For a modeling of concentrated colloidal nanoparticles, it is also important to treat accurately the contact interaction and the DLVO interaction [44] between the nanoparticles as well as the hydrodynamic interaction. The DLVO interaction consists of electrostatic potential and van der Waals potential that are exerted on a pair of colloidal nanoparticles. The magnitude of potentials depends strongly on the intersurface distance of the nanoparticles, so that it is crucial to evaluate accurately the intersurface distance of the particles. The contact interaction between colloidal nanoparticles plays a significant role when the nanoparticles aggregate, because the hydrodynamic interaction is less effective than the contact interaction inside agglomerates of the nanoparticles. The contact interaction is naturally shape sensitive, so that an accurate modeling of the nanoparticle shape is required. The authors aim to develop a simulation model that is suitable for investigating self-organization of concentrated colloidal nanoparticles in a flow, in which an applicable scope, a robustness, and an efficiency of the model should be taken into consideration as well as an accuracy. Desirable features of the model are as follows: (i) capability to solve a moderate Reynolds number flow that does not ensure the approximation of Stokes flow, (ii) capability to apply to a complicated flow geometry that contains solid walls, (iii) robustness for aggregated systems where nanoparticles frequently collide with one another, (iv) high computational efficiency for a large number of degree of freedom.

On the basis of above discussion, this paper presents an off-lattice–on-lattice hybrid simulation model. The translational motion and the rotational motion of nanoparticles are treated by the off-lattice Newtonian dynamics. The flow of solvent is treated by the on-lattice fluctuating Navier-Stokes equation. A fictitious domain (FD) method is employed to couple explicitly the motion of nanoparticles with the flow of solvent. The surface of the nanoparticle is expressed by discontinuous solid-liquid boundary to calculate accurately the contact interaction and the DLVO interaction between the nanoparticles. At the same time, the surface of the nanoparticle is expressed by continuous solid-liquid boundary to calculate efficiently hydrodynamic interaction. The contact interaction is evaluated according to the Voigt model [45–47], in which both elastic and viscous repulsions are included in the tangential direction as well as in the normal direction. The fluctuating Navier-Stokes equation is discretized to a

finite volume expression that is solved by the SIMPLEST (semi-implicit method for pressure-linked equations shortened) [48] that is an efficient variant of the SIMPLE [49]. The pressure in the particles is fixed to zero when the entire pressure field is solved. The present model includes all crucial forces and torques, such as contact force and torque, van der Waals force, electrostatic force, and hydrodynamic force and torque including thermal fluctuation of the solvent. In contrast to BSD, the present model can apply to a moderate Reynolds number flow where hydrodynamic inertial effects remain. The treatment of a no-slip wall is subtle in the models that treat a liquid as an ensemble of particles, such as DPD, LB, and SRD, whereas the boundary condition of a no-slip wall is reasonably introduced into the present model in such a manner as conventional Navier-Stokes simulation. Simulations of aggregated systems have some difficulties since a liquid is squeezed in small gaps between nanoparticles in contact with one another. In fact, some models that have discontinuous solid-liquid boundary, such as BSD and LB, have auxiliary devices to avoid a numerical instability [11,33]. In contrast, the present model that has continuous solid-liquid boundary is very robust for aggregated systems. Unlike DLMFD and FPD, separate time steps can be used for the motion of particles and the flow of solvent in the present model. In addition, the implicit temporal scheme can be adopted to evolve the flow field, unlike DPD, LB, and SRD. Furthermore, the pressure fix in the particle domain can accelerate the convergence of pressure field. Thus the present simulation model has a higher computational efficiency than other models. In fact, for a fixed computational domain, the computational cost of the present model is constant regardless of the concentration of colloidal nanoparticles. In contrast to the present model, a computational cost of the efficient BSD [12] that is a typical off-lattice model increases in $O(N \ln N)$ (N being the number of particles in the computational domain) to calculate the multibody hydrodynamic interaction. Computational costs of DPD and other off-lattice–on-lattice hybrid models in which only local hydrodynamic interactions are calculated increase as N, because the number of evaluations of the particle-to-particle interactions increases as N. The high computational efficiency is a fascinating novelty of the present simulation model. Although some authors have ever presented off-lattice–on-lattice hybrid models that contain the fluctuating Navier-Stokes equation with the IB method [21,22], their focuses are limited to the hydrodynamic interaction between particles and a liquid, whereas, the present model takes all crucial interactions into consideration.

The present simulation model is an upgrade of the previous model by the authors [51]. The previous model has contained the nonfluctuating Stokes equation with the IB method, in which the Brownian motion of nanoparticles has been induced by the stochastic force in the Newtonian dynamics of the nanoparticles. The fluctuation-dissipation theorem has not been strictly satisfied since the model employs the variance of stochastic force that is exerted on an isolated nanoparticle. The efficiency of the previous model has been relatively low since the temporal scheme to solve the Stokes equation is the explicit HSMAC (highly simplified marker and cell) [51]. In contrast, the present model satisfies the fluctuation-dissipation theorem and has much higher efficiency than the previous model. The purpose of this paper is to present a simulation model of concentrated colloidal nanoparticulate flows to investigate self-organization of nanoparticles and rheology of the colloid. In Sec. II, the present off-lattice–on-lattice hybrid simulation model is described. The discretization of equations and the solution algorithm are also given in detail. In Sec. III, some simulation results are illustrated to stress the capability of the present model. Finally, the conclusions of this paper are stated in Sec. IV.

II. SIMULATION MODEL

A. Motion of nanoparticles

The motion of solid nanoparticles is treated by the off-lattice Newtonian dynamics. A nanoparticle is assumed to be a rigid spherical body. The translational motion of the kth particle is expressed by

$$m_k \frac{d\boldsymbol{V}_k}{d\tau} = \boldsymbol{F}_k^{\mathrm{c}} + \boldsymbol{F}_k^{\mathrm{D}} + \boldsymbol{F}_k^{\mathrm{h}}, \tag{1}$$

where τ is time, m_k is the mass of the particle, $\boldsymbol{V}_k$ is the translational velocity of the particle, $\boldsymbol{F}_k^{\mathrm{c}}$ is the contact force, $\boldsymbol{F}_k^{\mathrm{D}}$ is the DLVO force that consists of electrostatic force and van der Waals force, and $\boldsymbol{F}_k^{\mathrm{h}}$ is the stochastic hydrodynamic force. Gravity force is negligible since the magnitude of force is much smaller than the above forces for colloidal nanoparticles. The trajectory of the kth particle is obtained from the translational velocity as

$$\frac{d\boldsymbol{X}_k}{d\tau} = \boldsymbol{V}_k, \tag{2}$$

where $\boldsymbol{X}_k$ denotes the center of the particle. The rotational motion of the kth particle is expressed by

$$I_k \frac{d\Omega_k}{d\tau} = \boldsymbol{T}_k^{\mathrm{c}} + \boldsymbol{T}_k^{\mathrm{h}}, \tag{3}$$

where I_k is the inertial moment of the particle, Ω_k is the angular velocity of the particle, $\boldsymbol{T}_k^{\mathrm{c}}$ is the contact torqu, and $\boldsymbol{T}_k^{\mathrm{h}}$ is the stochastic hydrodynamic torque.

In the existing simulation models, as far as the authors know, the contact interaction is treated by a simple elastic repulsion [16,26,28,42,52,53] or the Lennard-Jones potential [29,40]. These treatments are introduced just to avoid unphysical overlaps between particles in contact. On the other hand, the authors have shown that aggregation of colloidal nanoparticles is strongly affected by the contact interaction in the tangential direction (friction) between nanoparticles [50]. Therefore the present model employs a more sophisticated model of contact interaction. When the contact interaction is obtained, the discontinuous solid-liquid boundary is used to calculate accurately an intersurface distance between the particles. The contact force and the contact torque that are exerted on the kth particle are obtained by the summation as

$$\boldsymbol{F}_k^{\mathrm{c}} = \sum_l (\boldsymbol{F}_{kl}^{\mathrm{c,n}} + \boldsymbol{F}_{kl}^{\mathrm{c,t}}), \tag{4}$$

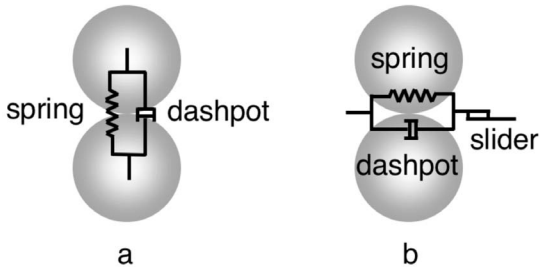

FIG. 1. Voigt model of contact interaction: (a) normal contact force; (b) tangential contact force.

$$\boldsymbol{T}_k^{\mathrm{c}} = \sum_l (a_k \boldsymbol{n}_{kl} \times \boldsymbol{F}_{kl}^{\mathrm{c,t}}), \tag{5}$$

where l denotes a particle that is in contact with the kth particle, $\boldsymbol{F}_{kl}^{\mathrm{c,n}}$ is the normal contact force between the kth particle and the lth particle, $\boldsymbol{F}_{kl}^{\mathrm{c,t}}$ is the tangential contact force between the kth particle and the lth particle, a_k is the radius of particle, $\boldsymbol{n}_{kl}$ is the unit vector from the center of the kth particle to the center of the lth particle.

Generally, colloidal nanoparticles at room temperature may be an elastic material rather than a viscoelastic material. A perfect elastic material, however, is an ideal, and all materials have the viscosity to some extent in addition to the elasticity. From this point of view, the Voigt model [45–47] is employed to resolve the contact force and the contact torque, as shown in Fig. 1. The normal and the tangential contact forces are given by the combination of elastic force and damping force as

$$\boldsymbol{F}_{kl}^{\mathrm{c,n}} = -k_{\mathrm{n}} \delta_{kl}^{\mathrm{n}\,3/2} \boldsymbol{n}_{kl} - \eta_{\mathrm{n}} (\boldsymbol{V}_{kl}^{\mathrm{r}} \cdot \boldsymbol{n}_{kl}) \boldsymbol{n}_{kl}, \tag{6}$$

$$\boldsymbol{F}_{kl}^{\mathrm{c,t}} = -k_{\mathrm{t}} \delta_{kl}^{\mathrm{t}} - \eta_{\mathrm{t}} \boldsymbol{V}_{kl}^{\mathrm{t}}, \tag{7}$$

where

$$\boldsymbol{V}_{kl}^{\mathrm{t}} = \boldsymbol{V}_{kl}^{\mathrm{r}} - (\boldsymbol{V}_{kl}^{\mathrm{r}} \cdot \boldsymbol{n}_{kl}) \boldsymbol{n}_{kl} + (a_k \Omega_k + a_l \Omega_l) \times \boldsymbol{n}_{kl}, \tag{8}$$

k_{n} is the elastic coefficient in the normal direction, k_{t} is the elastic coefficient in the tangential direction, η_{n} is the damping coefficient in the normal direction, η_{t} is the damping coefficient in the tangential direction, δ_{kl}^{n} is the normal relative displacement of the contact point, δ_{kl}^{t} is the tangential relative displacement of the contact point, and $\boldsymbol{V}_{kl}^{\mathrm{r}}$ is the relative velocity of the contact point. The tangential relative displacement of the contact point at time τ is derived from rotation of that at time $\tau - \Delta\tau$ and tangential relative velocity $\boldsymbol{V}_{kl}^{\mathrm{t}}$ as

$$\delta_{kl}^{\mathrm{t}}(\tau) = |\delta_{kl}^{\mathrm{t}}(\tau - \Delta\tau)| \frac{\boldsymbol{n}_{kl} \times \delta_{kl}^{\mathrm{t}}(\tau - \Delta\tau) \times \boldsymbol{n}_{kl}}{|\boldsymbol{n}_{kl} \times \delta_{kl}^{\mathrm{t}}(\tau - \Delta\tau) \times \boldsymbol{n}_{kl}|} + \boldsymbol{V}_{kl}^{\mathrm{t}} \Delta\tau, \tag{9}$$

because the unit normal vector to the contact plane changes the direction during $\Delta\tau$. According to the law of Coulomb friction, a slip occurs at the contact point if $|\boldsymbol{F}_{kl}^{\mathrm{c,t}}| \geq \mu |\boldsymbol{F}_{kl}^{\mathrm{c,n}}|$, and the tangential relative displacement is modified as

$$\delta_{kl}^{\mathrm{t}} = -\boldsymbol{F}_{kl}^{\mathrm{c,t}} / k_{\mathrm{t}}, \tag{10}$$

where

$$\boldsymbol{F}_{kl}^{\mathrm{c,t}} = -\mu |\boldsymbol{F}_{kl}^{\mathrm{c,n}}| \frac{\boldsymbol{V}_{kl}^{\mathrm{t}}}{|\boldsymbol{V}_{kl}^{\mathrm{t}}|}, \tag{11}$$

μ is the frictional coefficient between the particles. The elastic coefficient in the normal direction is given by the Hertzian contact theory [54], and the elastic coefficient in the tangential direction is determined from the Mindlin model [55]. The normal and the tangential damping coefficients are assumed to be the same value.

The damping coefficients can be obtained from the coefficient of restitution of particles [46]. The previous experiments [56,57] have shown that the coefficient of restitution is not constant but depends sensitively on the relative velocity between the particles just before a contact. Although some rigorous theoretical formulas of the coefficient of restitution have been proposed [58,59], using the formulas for each collision between the particles is so expensive that a computational efficiency of the present model is degraded. Since we do not aim to describe the evolution of each collision of the particles in detail but aim to describe the structure of aggregated nanoparticles, the coefficient of restitution is determined in terms of numerical stability. In fact, a perfect elastic model of the contact interaction where the coefficient of restitution is 1 sometimes leads to a numerical instability on the motion of particles, because an excessive overlap between the particles due to a finite time step gives an unphysical elastic repulsive force. To avoid the excessive overlap between the particles, the damping coefficients are given so that the restitution coefficient is 0.2 here. As it will be described later, the lubrication force that is exerted between a pair of particles approaching each other can be underestimated in the present model of hydrodynamic force. If the lubrication force would be exactly estimated, a pure elastic model of the contact interaction might work well because the relative velocity between the particles could be attenuated before the contact of particles and no excessive overlap could occur. It can be said that the present model adopts the Voigt model instead of the exact lubrication force in order to stabilize the contact between the particles. On the other hand, we would emphasize that the contact interaction in the tangential direction (friction) between the particles is more important than the contact interaction in the normal direction for aggregation of nanoparticles. The present model including the friction between the nanoparticles has a capability to reproduce more accurately the structure of aggregated colloidal nanoparticles.

The DLVO force is a function of an intersurface distance between particles that have the discontinuous solid-liquid boundary. The force that is exerted on the kth particle is given as

$$\boldsymbol{F}_k^{\mathrm{D}} = \sum_l (f_{kl}^{\mathrm{e}} + f_{kl}^{\mathrm{v}}) \boldsymbol{n}_{kl}, \tag{12}$$

where l denotes the particle around the kth particle. The magnitude of two-body electrostatic force f_{kl}^{e} is given by the

DLVO theory [45] by way of Derjaguin's approximation [45] as

$$f_{kl}^{e} = -\frac{64\pi\bar{a}_{kl}nk_BT\Theta_k\Theta_l e^{-\kappa H_{kl}}}{\kappa}, \tag{13a}$$

where

$$\bar{a}_{kl} = \frac{2a_k a_l}{a_k + a_l}, \tag{13b}$$

$$\Theta_k = \tanh\left(\frac{ze\varphi_k}{4k_BT}\right), \tag{13c}$$

$$\kappa = \sqrt{\frac{2nz^2e^2}{\epsilon_0\epsilon_r k_BT}}, \tag{13d}$$

n is the number of density of electrolyte ions in the solvent whose electrolyte ionic valency is z, k_B is the Boltzmann constant, T is the temperature of the solvent, H_{kl} is the intersurface distance between the kth particle and the lth particle, e is the elementary electric charge, φ_k is the zeta potential of the kth particle, ϵ_0 is the permittivity of vacuum, and ϵ_r is the relative permittivity of the solvent. The magnitude of two-body van der Waals force f_{kl}^{v} is also given by the DLVO theory by way of a volume integration of the forces that are exerted between atoms in the particles as

$$f_{kl}^{v} = \frac{A\bar{a}_{kl}}{12H_{kl}^2}, \tag{14}$$

where A is the Hamaker constant. Note that the magnitude of the van der Waals force is limited below a maximum value to avoid a divergence when the intersurface distance comes to zero. The expressions of the stochastic hydrodynamic force and torque will be described subsequently.

B. Flow field

The nanoparticles are embedded on a Cartesian lattice in a computational domain. The entire flow field that contains both the particle domain and the solvent domain is treated by the fluctuating Navier-Stokes equation [18–20]. with the fictitious domain (FD) method [26–28]. The incompressibility condition of the flow field is given as

$$\nabla \cdot \boldsymbol{u} = 0, \tag{15}$$

where $\boldsymbol{u}$ is the velocity on the lattice. The momentum equation is expressed by

$$\frac{\partial \boldsymbol{u}}{\partial t} + \boldsymbol{u}\cdot\nabla\boldsymbol{u} = -\frac{1}{\rho}\nabla p + \nu\nabla^2\boldsymbol{u} + \frac{1}{\rho}\nabla\cdot\boldsymbol{S} + \Phi\boldsymbol{\alpha}, \tag{16a}$$

where

$$\boldsymbol{\alpha} = \frac{\boldsymbol{u}^{\mathrm{p}} - \boldsymbol{u}}{\Delta t} + \frac{1}{\rho}\nabla p + \boldsymbol{u}\cdot\nabla\boldsymbol{u} - \nu\nabla^2\boldsymbol{u} - \frac{1}{\rho}\nabla\cdot\boldsymbol{S}, \tag{16b}$$

t is time, ρ is the density of solvent, p is the pressure, ν is the dynamic viscosity of the solvent, $\boldsymbol{S}$ is the fluctuating stress tensor, Φ is the volume fraction of the particles, and $\boldsymbol{u}^{\mathrm{p}}$ is the particle velocity on the lattice. The fluctuating stress tensor is the stochastic term whose components give [21]

$$\langle S_{ij}(\boldsymbol{r},t)\rangle = 0,$$

$$\langle S_{ik}(\boldsymbol{r}_1,t_1)S_{lm}(\boldsymbol{r}_2,t_2)\rangle = 2k_BT\eta(\delta_{il}\delta_{km} + \delta_{im}\delta_{kl})\delta(\boldsymbol{r}_1 - \boldsymbol{r}_2) \times \delta(t_1 - t_2), \tag{17}$$

where $\boldsymbol{r}$ is position, $\langle\ \rangle$ denotes averaging over an ensemble, η is the viscosity of the solvent, δ_{ij} is the Kronecker's delta, and $\delta(\ )$ is the Dirac delta function. In two dimensions, Eq. (17) is written as

$$\langle S_{xx}\rangle = \langle S_{yy}\rangle = \langle S_{xy}\rangle = \langle S_{yx}\rangle = 0,$$

$$\langle S_{xx}^2\rangle = \langle S_{yy}^2\rangle = 4k_BT\eta\delta(\Delta x)\delta(\Delta y)\delta(\Delta t),$$

$$\langle S_{xy}^2\rangle = \langle S_{yx}^2\rangle = 2k_BT\eta\delta(\Delta x)\delta(\Delta y)\delta(\Delta t), \tag{18}$$

where Δx and Δy are spacings of the lattice and Δt is a time step. Equation (18) shows that components of the fluctuating stress tensor obey Gaussian distributions with the mean of zero. The volume fraction of the particles Φ is a summation of the volume fraction of each particle as

$$\Phi = \sum_k \phi_k(\boldsymbol{r}). \tag{19}$$

For spherical particles, the volume fraction of the kth particle can be given by a hyperbolic tangent function [29,60] as

$$\phi_k(\boldsymbol{r}) = \frac{1}{2}\left\{\tanh\left(\frac{a_k - |\boldsymbol{r} - \boldsymbol{r}_k|}{\zeta}\right) + 1\right\}, \tag{20}$$

where $\boldsymbol{r}_k$ is the center of the kth particle and ζ determines the thickness of a solid-liquid boundary. The value of Eq. (20) smoothly changes from 0 to 1 through the surface of the particle, so that the present model has a continuous solid-liquid boundary on the lattice. ζ is 0.025, so that the thickness of the boundary is represented by twice the lattice spacing. The particle velocity $\boldsymbol{u}^{\mathrm{p}}$ on the lattice is a summation of the rigid velocity of each particle as

$$\Phi\boldsymbol{u}^{\mathrm{p}} = \sum_k \{\phi_k(\boldsymbol{r})[\boldsymbol{V}_k + (\boldsymbol{r} - \boldsymbol{r}_k)\times\Omega_k]\}. \tag{21}$$

$\boldsymbol{\alpha}$ in Eqs. (16a) and (16b) is the stochastic acceleration term to force the rigid velocity of particles on the lattice. In the solvent domain where $\Phi=0$, Eqs. (16a) and (16b) reduces to the fluctuating Navier-Stokes equation. In the particle domain where $\Phi=1$, Eqs. (16a) and (16b) becomes

$$\frac{\partial \boldsymbol{u}}{\partial t} = \frac{\boldsymbol{u}^{\mathrm{p}} - \boldsymbol{u}}{\Delta t}. \tag{22}$$

If a single-step temporal scheme is adopted, the velocity at the next time step is automatically set to the particle velocity without the fluctuation. The present FD method does not require any additional operation to impose the boundary condition at the surface of particles, unlike the IB method. The counteraction of the stochastic acceleration term is exerted on a unit volume of the particles, so that the hydrodynamic

force and torque in Eqs. (1) and (3) are estimated by a volume integration as

$$\boldsymbol{F}_k^{\mathrm{h}} = -\int \phi_k(\boldsymbol{r})\rho\boldsymbol{\alpha}(\boldsymbol{r})d\boldsymbol{r}, \tag{23}$$

$$\boldsymbol{T}_k^{\mathrm{h}} = -\int \phi_k(\boldsymbol{r})\{(\boldsymbol{r}-\boldsymbol{r}_k)\times\rho\alpha(\boldsymbol{r})\}d\boldsymbol{r}, \tag{24}$$

where the integration is carried out in a whole particle. Equations (23) and (24) represent that the continuous solid-liquid boundary is used to calculate the hydrodynamic force and torque exerted on the particles. Note that the translational and rotational Brownian motions of the particles emanate from the above stochastic hydrodynamic force and torque.

When two particles approach each other and the intersurface distance between the particles is of the order of a lattice spacing, Eqs. (23) and (24) cannot exactly resolve the lubrication interaction between the particles. The drawback is not due to the continuous solid-liquid boundary, but is essentially due to the discretization of fluid on a lattice. Even if a discontinuous solid-liquid boundary is imposed on the lattice, the no-slip condition on the solid-liquid boundary is given by an interpolative manner because the boundary does not always coincide with the lattice. Namely, the solid-liquid boundary is diffused. Thus the drawback is a problem that is encountered by all off-lattice–on-lattice hybrid models. A pair of particles approaching each other may easily contact due to an underestimate of the repulsive lubrication force in the present model, whereas actual particles may hardly contact and the relative velocity between the particles rapidly decreases due to the lubrication force. In the case of nanoparticles, nevertheless, the actual particles contact each other after all, because the interparticle attractive interaction (van der Waals force) significantly affects particles in the vicinity. Consequently, it is considered that the present model is able to reproduce aggregation of concentrated colloidal nanoparticles in spite of an error of the lubrication interaction. It is naturally possible to evaluate the lubrication interaction accurately by use of the analytical solution [61–63] when two particles come close within the order of a lattice spacing.

Since the particles are assumed to be rigid, there may be binary distributions of pressure in the particle domain. The first component is a linear distribution of pressure in the traveling direction that is associated with a translational accelerated motion of particle. The second component is a centrally symmetric linear distribution of pressure in the radial direction that is associated with a rotational motion of particle. The total pressure difference in the particle domain due to the linear distribution in the traveling direction exerts a force on the particle, but does not exert any torque. On the other hand, the centrally symmetric linear distribution of pressure in the radial direction exerts neither force nor torque on the particle. As shown in Fig. 2, the linear distribution of pressure in the traveling direction can be replaced with an arbitrary constant pressure in the particle domain, because this replacement does not change the total pressure difference Δp that is reproduced at the particle boundary. Therefore pressure distribution in the particle domain can be fixed

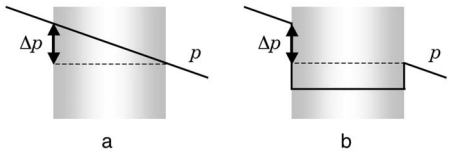

FIG. 2. Pressure fix in particle domain: (a) linear pressure distribution; (b) constant pressure distribution.

to an arbitrary constant without influence on the motion of particle. In addition, the flow field in the solvent domain is determined by the velocity at the surface of particles regardless of pressure in the particle domain. Based on the above statement, pressure in the particle domain is fixed to zero as

$$p = 0 \quad \text{if} \quad \Phi = 1. \tag{25}$$

This pressure fix in the particle domain can increase the stability of time evolution and accelerate convergence of the pressure field as the particle concentration increases.

C. Discretization of equations

The forces and torques exerted on a nanoparticle have different characteristic times. The characteristic times of $\boldsymbol{F}^{\mathrm{c}}$ and $\boldsymbol{F}^{\mathrm{D}}$ in Eq. (1) and $\boldsymbol{T}^{\mathrm{c}}$ in Eq. (3) are associated with the motion of molecules. The characteristic times of $\boldsymbol{F}^{\mathrm{h}}$ in Eq. (1) and $\boldsymbol{T}^{\mathrm{h}}$ in Eq. (3), on the other hand, are associated with the motion of nanoparticle. The former characteristic times are typically smaller than the latter characteristic times. The FD method in the present simulation model can separate the time evolution of particle motion from the time evolution of flow field since both time evolutions are explicitly coupled with each other, unlike the DLMFD method. Therefore a small time step $\Delta\tau$ is used to evaluate $\boldsymbol{F}^{\mathrm{c}}$, $\boldsymbol{F}^{\mathrm{D}}$, and $\boldsymbol{T}^{\mathrm{c}}$, and a large time step Δt is used to evaluate $\boldsymbol{F}^{\mathrm{h}}$ and $\boldsymbol{T}^{\mathrm{h}}$. This dual time stepping saves the computational cost since the evaluation of $\boldsymbol{F}^{\mathrm{h}}$ and $\boldsymbol{T}^{\mathrm{h}}$ requires rather expensive calculation of the flow field. The relation of $\Delta\tau$ and Δt is given as

$$\Delta t = l_{\max}\Delta\tau, \tag{26}$$

where $l_{\max}$ is a positive integer. Figure 3 shows the dual time

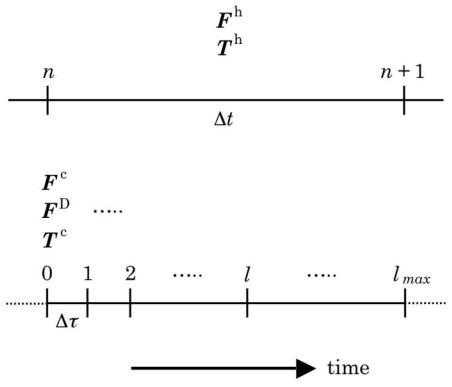

FIG. 3. Dual time stepping to evaluate forces and torques exerted on nanoparticle.

stepping to evaluate forces and torques that are exerted on a nanoparticle. $\boldsymbol{F}^{\mathrm{c}}$, $\boldsymbol{F}^{\mathrm{D}}$, and $\boldsymbol{T}^{\mathrm{c}}$ are evaluated at each $\Delta\tau$. $\boldsymbol{F}^{\mathrm{h}}$ and $\boldsymbol{T}^{\mathrm{h}}$ are evaluated at each Δt. In other words, the time step to solve the particle motion is $\Delta\tau$, and the time step to solve the flow field is Δt.

The translational and rotational motions of particles are solved by the first-order Euler explicit scheme. Equation (1) and Eq. (3) are temporally discretized as

$$\boldsymbol{V}_k^{l+1} = \boldsymbol{V}_k^l + \frac{\Delta\tau}{m_k}(\boldsymbol{F}_k^{\mathrm{c}^l} + \mathbf{F}_k^{\mathrm{D}^l} + \mathbf{F}_k^{\mathrm{h}^{n+1/2}}), \tag{27}$$

$$\Omega_k^{l+1} = \Omega_k^l + \frac{\Delta\tau}{I_k}(\boldsymbol{T}_k^{\mathrm{c}^l} + \boldsymbol{T}_k^{\mathrm{h}^{n+1/2}}), \tag{28}$$

where l and n denote discrete times in Fig. 3. Equation (2) is temporally discretized by the Crank-Nicolson scheme as

$$\boldsymbol{X}_k^{l+1} = \boldsymbol{X}_k^l + \frac{\Delta\tau}{2}(\boldsymbol{V}_k^l + \boldsymbol{V}_k^{l+1}). \tag{29}$$

One can use a second-order scheme for Eqs. (1)–(3), such as a Runge-Kutta or the predictor-corrector velocity Verlet [64].

The lattice spacing is about a tithe of the size of a nanoparticle to resolve the flow in the small gap between the nanoparticles in a concentrated colloid. Such a small lattice spacing requires a prohibitively small time step to solve with stability the momentum equation of flow by an explicit scheme. The present model adopts the Crank-Nicolson implicit scheme for the convective term and the diffusive term in the momentum equation. The scheme is suitable for time evolution simulations since it has second-order accuracy with time. Equations (16a) and (16b) is temporally discretized as

$$\frac{\boldsymbol{u}^{n+1} - \boldsymbol{u}^n}{\Delta t} + \frac{1}{2}(\boldsymbol{u}^{n+1}\cdot\nabla\boldsymbol{u}^{n+1} - \nu\nabla^2\boldsymbol{u}^{n+1}) = -\frac{1}{2}(\boldsymbol{u}^n\cdot\nabla\boldsymbol{u}^n - \nu\nabla^2\boldsymbol{u}^n) - \frac{1}{\rho}\nabla p^{n+1} + \frac{1}{\rho}\nabla\cdot\boldsymbol{S}^{n+1/2} + \Phi^n\boldsymbol{\alpha}^{n+1/2}, \tag{30a}$$

where

$$\boldsymbol{\alpha}^{n+1/2} = \frac{\boldsymbol{u}^{\mathrm{p}^n} - \boldsymbol{u}^n}{\Delta t} + \frac{1}{\rho}\nabla p^{n+1} + \frac{1}{2}(\boldsymbol{u}^{n+1}\cdot\nabla\boldsymbol{u}^{n+1} - \nu\nabla^2\boldsymbol{u}^{n+1}) + \frac{1}{2}(\boldsymbol{u}^n\cdot\nabla\boldsymbol{u}^n - \nu\nabla^2\boldsymbol{u}^n) - \frac{1}{\rho}\nabla\cdot\boldsymbol{S}^{n+1/2}, \tag{30b}$$

$n+1/2$ denotes the intermediate time between n and $n+1$. The fluctuating stress term $\boldsymbol{S}$ can be obtained at an arbitrary time since the term has no time correlation. If the volume fraction of particles Φ and the particle velocity $\boldsymbol{u}^{\mathrm{p}}$ are known at the time n, Eqs. (30a) and (30b) leads to a system of equations for unknown $\boldsymbol{u}^{n+1}$ and p^{n+1}. On the other hand, Eq. (15) is temporally discretized as

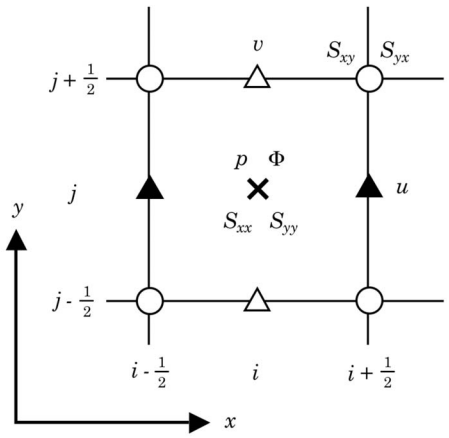

FIG. 4. Staggered arrangement of flow variables on two-dimensional (2D) uniform Cartesian lattice.

$$\nabla\cdot\boldsymbol{u}^{n+1} = 0. \tag{31}$$

Equations (30a), (30b), and (31) can be solved by a pressure-velocity coupling method.

The present simulation model employs a finite volume method on a uniform Cartesian lattice together with a staggered arrangement of the flow variables. Figure 4 shows the arrangement of flow variables on a two-dimensional lattice. A pair of indices (i,j) denotes a cell center and $\pm 1/2$ denotes the cell edges. p, Φ, S_{xx}, and S_{yy} are evaluated at the cell center ($\times$). The velocity components u and v are evaluated at the center of cell edges ($\blacktriangle$,$\triangle$). S_{xy} and S_{yx} are evaluated at the cell vertices ($\bigcirc$). The above arrangement of flow variables ensures the conservation law of mass and momentum. The volume fraction Φ at cell edges are required when Eqs. (30a) and (30b) is evaluated. They are obtained by simple arithmetic average of the values at the cell centers in both sides. All spatial derivatives of Eqs. (30a), (30b), and (31) are approximated by a central difference scheme. Any upwind difference scheme is not necessary to approximate the convective terms in Eqs. (30a) and (30b), because the Reynolds number of the present nanoparticulate flows is sufficiently small. Equation (18) is discretized as

$$\langle S_{xx}^2\rangle = \langle S_{yy}^2\rangle = \frac{4k_BT\eta}{\Delta x\Delta y\Delta t},$$

$$\langle S_{xy}^2\rangle = \langle S_{yx}^2\rangle = \frac{2k_BT\eta}{\Delta x\Delta y\Delta t}, \tag{32}$$

where Δx and Δy are the lattice spacing in the x direction and in the y direction, respectively. Consequently, the spatially discretized expression of Eqs. (30a) and (30b) in two dimensions is given as the system of algebraic equations

$$u_{i\pm1/2,j}^{n+1} = \frac{\sum_{nb} a_{nb}^u u_{nb}^{n+1} + b_{i\pm1/2,j}^u}{a_{i\pm1/2,j}^u} - (1-\Phi_{i\pm1/2,j}^n) \times \frac{\pm p_{i\pm1,j}^{n+1} \mp p_{i,j}^{n+1}}{a_{i\pm1/2,j}^u \Delta x}, \tag{33}$$

$$v_{i,j\pm\frac{1}{2}}^{n+1} = \frac{\sum_{nb} a_{nb}^{v} v_{nb}^{n+1} + b_{i,j\pm 1/2}^{v}}{a_{i,j\pm 1/2}^{v}} - (1 - \Phi_{i,j\pm 1/2}^{n}) \times \frac{\pm p_{i,j\pm 1}^{n+1} \mp p_{i,j}^{n+1}}{a_{i,j\pm 1/2}^{v} \Delta y}, \tag{34}$$

where $\pm$ and $\mp$ are used in the same order, nb denotes four neighbors of the point at which each equation is evaluated. The coefficients b^u and b^v that are functions of the variables at n and $n+1/2$ step are constant in the above equations. The coefficients a^u and a^v, on the other hand, are functions of unknown u^{n+1} and v^{n+1}, respectively, because the convective terms in Eq. (30a) and (30b) are nonlinear. Equation (31) is spatially discretized as

$$\frac{u_{i+1/2,j}^{n+1} - u_{i-1/2,j}^{n+1}}{\Delta x} + \frac{v_{i,j+1/2}^{n+1} - v_{i,j-1/2}^{n+1}}{\Delta y} = 0, \tag{35}$$

where the subscripts are synonymous with Eqs. (33) and (34).

D. Solution algorithm

An iterative algorithm is required to solve Eqs. (33)–(35) since Eqs. (33) and (34) are nonlinear. The present simulation model uses the SIMPLEST (semi-implicit method for pressure-linked equations shortened) [48], that is known as one of the most efficient incompressible Navier-Stokes solvers. The authors dare to illustrate below the algorithm of SIMPLEST, because the algorithm has never, to our knowledge, been applied to the fluctuating Navier-Stokes equation with the FD method in the literature. In two dimensions, the algorithm to evolve the flow field from n step to $n+1$ step is given as the following steps:

1. Evaluate $S_{xx}^{n+1/2}$, $S_{yy}^{n+1/2}$, $S_{xy}^{n+1/2}$, and $S_{yx}^{n+1/2}$ using Eq. (32) and calculate b^u and b^v in Eqs. (33) and (34).

2. Set initial guesses of the velocity components as

$$u_{i\pm 1/2,j}^{m} = u_{i\pm 1/2,j}^{n},$$

$$v_{i,j\pm 1/2}^{m} = v_{i,j\pm 1/2}^{n}, \tag{36}$$

where m (=0) is the number of iterations.

3. Give pseudovelocity components using Eqs. (33) and (34) as

$$\hat{u}_{i\pm 1/2,j}^{m+1} = \frac{\sum_{nb} a_{nb}^{u,m} u_{nb}^{m} + b_{i\pm 1/2,j}^{u}}{a_{i\pm 1/2,j}^{u,m}} - (1 - \Phi_{i\pm 1/2,j}^{n}) \times \frac{\pm p_{i\pm 1,j}^{m+1} \mp p_{i,j}^{m+1}}{a_{i\pm 1/2,j}^{u,m} \Delta x}, \tag{37}$$

$$\hat{v}_{i,j\pm 1/2}^{m+1} = \frac{\sum_{nb} a_{nb}^{v,m} v_{nb}^{m} + b_{i,j\pm 1/2}^{v}}{a_{i,j\pm 1/2}^{v,m}} - (1 - \Phi_{i,j\pm 1/2}^{n}) \times \frac{\pm p_{i,j\pm 1}^{m+1} \mp p_{i,j}^{m+1}}{a_{i,j\pm 1/2}^{v,m} \Delta y}, \tag{38}$$

where coefficients $a^{u,m}$ and $a^{v,m}$ denote the functions of u^m and v^m, respectively.

4. Substitute the pseudovelocity components with the velocity components in Eq. (35) as

$$\frac{\hat{u}_{i+1/2,j}^{m+1} - \hat{u}_{i-1/2,j}^{m+1}}{\Delta x} + \frac{\hat{v}_{i,j+1/2}^{m+1} - \hat{v}_{i,j-1/2}^{m+1}}{\Delta y} = 0. \tag{39}$$

The above equation is not satisfied during iterations.

5. Get the system of equations for tentative pressure using Eqs. (37)–(39) as

$$p_{i,j}^{m+1} = \frac{\sum_{nb} a_{nb}^{p,m} p_{nb}^{m+1} + b_{i,j}^{p,m}}{a_{i,j}^{p,m}}, \tag{40}$$

where the coefficient $a^{p,m}$ is the function of $a^{u,m}$ and $a^{v,m}$, and the coefficient $b^{p,m}$ is the function of $a^{u,m}$, $a^{v,m}$, b^u, b^v, u^m, and v^m.

6. Solve Eq. (40) to get $p_{i,j}^{m+1}$. The red-black SOR (successive over relaxation) method is used here for parallelization of the simulation code. The pressure fix of Eq. (25) and the boundary condition of pressure is imposed at each relaxation step. One can use a multigrid method [65] or a conjugate gradient type method [66] to solve Eq. (40).

7. Get tentative velocity components using $p_{i,j}^{m+1}$ as

$$u_{i\pm 1/2,j}^{m+1} = \frac{\sum_{nb} a_{nb}^{u,m} u_{nb}^{m} + b_{i\pm 1/2,j}^{u}}{a_{i\pm 1/2,j}^{u,m}} - (1 - \Phi_{i\pm 1/2,j}^{n}) \times \frac{\pm p_{i\pm 1,j}^{m+1} \mp p_{i,j}^{m+1}}{a_{i\pm 1/2,j}^{u,m} \Delta x}, \tag{41}$$

$$v_{i,j\pm 1/2}^{m+1} = \frac{\sum_{nb} a_{nb}^{v,m} v_{nb}^{m} + b_{i,j\pm 1/2}^{v}}{a_{i,j\pm 1/2}^{v,m}} - (1 - \Phi_{i,j\pm 1/2}^{n}) \times \frac{\pm p_{i,j\pm 1}^{m+1} \mp p_{i,j}^{m+1}}{a_{i,j\pm 1/2}^{v,m} \Delta y}. \tag{42}$$

The boundary condition of u^{m+1} and v^{m+1} are imposed.

8. If u^{m+1} and v^{m+1} are converged, the flow field at the next time step is obtained as

$$u_{i\pm 1/2,j}^{n+1} = u_{i\pm 1/2,j}^{m+1},$$

$$v_{i,j\pm 1/2}^{n+1} = v_{i,j\pm 1/2}^{m+1},$$

$$p_{i,j}^{n+1} = p_{i,j}^{m+1}. \tag{43}$$

Otherwise, substitute $m+1$ for m and return to step 3.

The motion of nanoparticles and the flow field are explicitly coupled with each other. In a word, the equations of nanoparticle motion and the equations of flow field are solved by turns at each time step. The whole solution algorithm of the present simulation model is given as the following steps:

1. Initialize $\boldsymbol{V}^n$, Ω^n, and $\boldsymbol{X}^n$ (n=0) for every nanoparticle.

2. Initialize $\boldsymbol{u}^n$ and p^n (n=0) in the entire computational domain.

3. Calculate ϕ^n at cell centers in the lattice using Eq. (20).

4. Calculate $\boldsymbol{u}^{\mathrm{p}^n}$ at cell edges in the lattice using Eq. (21).

5. Solve the flow field using the SIMPLEST to get $\boldsymbol{u}^{n+1}$ and p^{n+1} in the entire computational domain.

6. Calculate $\boldsymbol{\alpha}^{n+1/2}$ in the entire computational domain using Eq. (30b).

7. Calculate $\boldsymbol{F}^{\mathrm{h}^{n+1/2}}$ and $\boldsymbol{T}^{\mathrm{h}^{n+1/2}}$ for every nanoparticle using Eqs. (23) and (24).

8. Initialize $\boldsymbol{X}^l$, Ω^l, and $\boldsymbol{V}^l$ $(l=0)$ for every nanoparticle as

$$\boldsymbol{V}^l = \boldsymbol{V}^n,$$

$$\Omega^l = \Omega^n,$$

$$\boldsymbol{X}^l = \boldsymbol{X}^n. \tag{44}$$

9. Calculate $\boldsymbol{F}^{\mathrm{c}^l}$, $\boldsymbol{F}^{\mathrm{D}^l}$, and $\boldsymbol{T}^{\mathrm{c}^l}$ for every nanoparticle.

10. Solve the particle motion using Eqs. (27)–(29) to get $\boldsymbol{V}^{l+1}$, Ω^{l+1}, and $\boldsymbol{X}^{l+1}$ for every nanoparticle.

11. If $l+1=l_{\max}$, get the particle velocity and the particle position at the next time step as

$$\boldsymbol{V}^{n+1} = \boldsymbol{V}^{l+1},$$

$$\Omega^{n+1} = \Omega^{l+1},$$

$$\boldsymbol{X}^{n+1} = \boldsymbol{X}^{l+1}. \tag{45}$$

12. Otherwise, substitute $l+1$ for l and return to step 9.

13. Substitute $n+1$ for n and return to step 3.

III. SIMULATION RESULTS

The authors demonstrate the capability of the present simulation model by two-dimensional simulations where identical circular nanoparticles are contained in a square computational domain. The diameter of nanoparticles is $2a=50$ nm. The computational domain that has 240×240 uniform computational cells has a side length of $L=54a$. The zeta potential of nanoparticles is $\varphi=-40$ mV, and the frictional coefficient between the nanoparticles is $\mu=0.2$. Other physical and chemical properties of the nanoparticles and the solvent are given by the same values as polystyrene and water in normal temperature, respectively. The volume fraction of nanoparticles is $\phi=0.5$ to emphasize the capability of the present model for concentrated colloids. Hence the number of nanoparticles is $N_p=463$. In a subsequent description, simulation time is nondimensionalized as

$$t^* = \frac{t}{\tilde{t}}, \tag{46}$$

where t^* is nondimensional time, $\tilde{t}$ is a time during which a nanoparticle diffuses for a mean gap between the nanoparticles as

$$\tilde{t} = \frac{\sigma^2}{2D}, \tag{47}$$

where σ is the mean gap and $D=k_BT/6\pi\eta a$ is the self-diffusion coefficient of a nanoparticle. The mean gap is evaluated from the volume fraction as

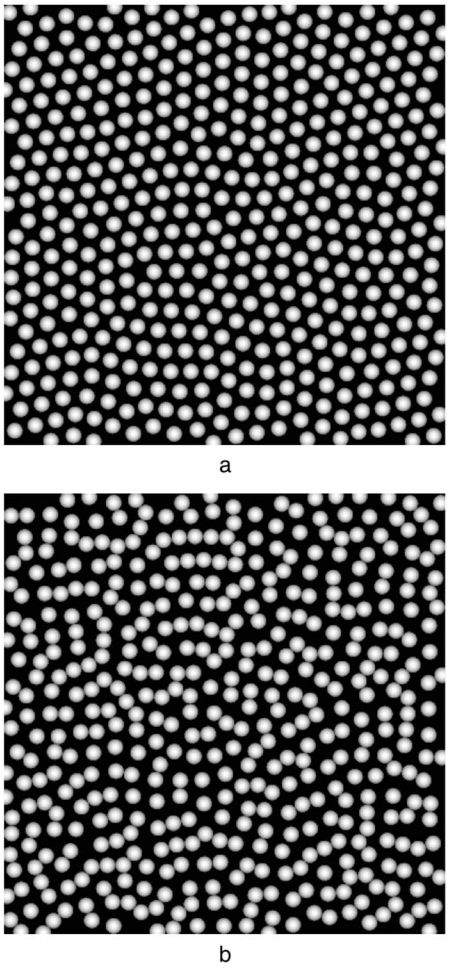

FIG. 5. Snapshots of self-organization simulation of still colloid: (a) $t^*=0$; (b) $t^*=3$.

$$\sigma = \left(\frac{\sqrt{2\pi}}{\sqrt[4]{3}} \frac{1}{\sqrt{\phi}} - 2 \right) a. \tag{48}$$

A. Self-organization of nanoparticles in a still colloid

First, a simulation of self-organization of the nanoparticles in a still colloid is presented to illustrate the balance of forces and torques that are exerted on a nanoparticle. The simulation has been carried out under the condition of periodic boundaries in all directions. Figure 5 shows snapshots of the simulation result. At $t^*=0$, the colloidal nanoparticles are completely dispersed in the computational domain. In $t^*=3$, the nanoparticles aggregate with one another and a labyrinthlike structure emanates throughout the domain. For a dilute system, colloidal nanoparticles with the zeta potential of -40 mV hardly aggregate because of the long-distance repulsive potential between the nanoparticles. For a concentrated system, in contrast, colloidal nanoparticles that have relatively high repulsive potential sometimes collide with one another since the displacement of nanoparticles by the Brownian motion can exceed the interparticle distance. Once a collision of nanoparticles occurs, the nanoparticles

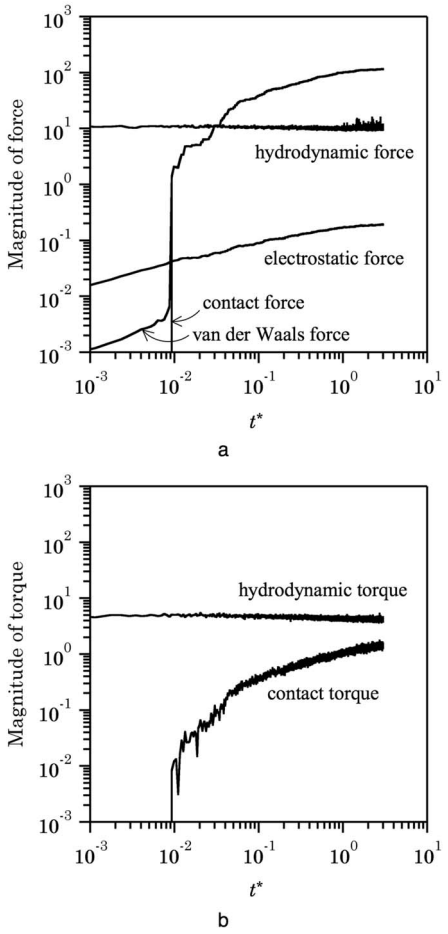

FIG. 6. Time history of magnitude of forces and torques exerted on nanoparticle in a still colloid: (a) force; (b) torque.

hardly detach from one another due to the strong van der Waals attractive force.

Figure 6 shows time history of the nondimensionalized magnitude of forces and torques exerted on a nanoparticle that are averaged over every nanoparticle. At the beginning of simulation, the magnitudes of contact force and contact torque are zero since no nanoparticle aggregates. At this time, the electrostatic force is larger than the van der Waals force since the interparticle distance is relatively large. The fluctuating hydrodynamic force is the primary force, and the fluctuating hydrodynamic torque is the only torque to be exerted on nanoparticles. Aggregation of the nanoparticles begins just after starting the simulation, so that the contact force and the contact torque emanates. At the same time, the magnitude of the van der Waals force rapidly increases since the interparticle distance decreases. The contact force and the van der Waals force have the same magnitude, and they become primary forces. In a word, the contact force acts as a counterbalance to the van der Waals force when the nanoparticles are in contact. As the aggregation of nanoparticles proceeds, the magnitude of contact torque approaches the magnitude of fluctuating hydrodynamic torque, because the contact torque acts as a counterbalance to the fluctuating hydrodynamic torque for nanoparticles in aggregates. As shown in Fig. 6, the balance of forces and torques that are exerted

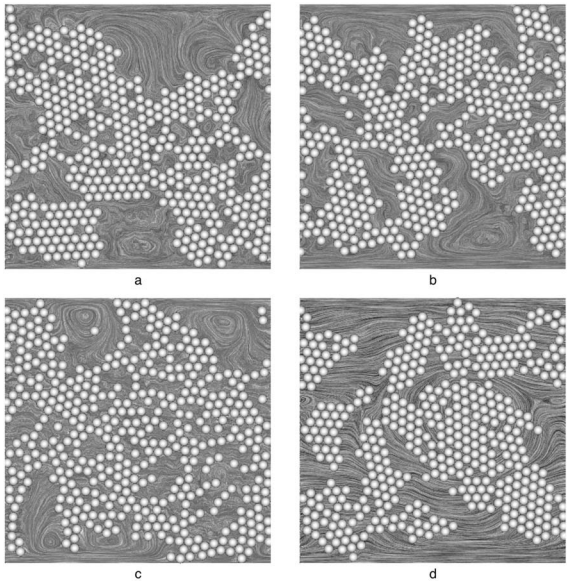

FIG. 7. Snapshots of self-organization simulation of colloidal nanoparticles in shear flows: (a) Pe=10; (b) Pe=10^2; (c) Pe=10^3; (d) Pe=10^4.

on a nanoparticle changes considerably during the simulation. Consequently, every force in the present simulation model should be taken into consideration for self-organization of concentrated colloidal nanoparticles.

B. Self-organization of nanoparticles in shear flows

The self-organization of concentrated colloidal nanoparticles in a shear flow is a major objective to which the present simulation model is applied. A nanoparticulate shear flow is characterized by the Péclet number as

$$\mathrm{Pe} = \frac{\dot{\gamma}\mathrm{a}^2}{\mathrm{D}}, \tag{49}$$

where $\dot{\gamma}=U/L$ is the shear rate. To yield a simple shear field, the top and bottom boundaries of the computational domain are assumed to be solid walls that move in the x direction at the velocity of $U/2$ and $-U/2$, respectively. The periodic boundary condition is imposed in the horizontal direction. A preliminary simulation of the still colloid (Pe=0) is enforced to generate the initial condition where the colloidal nanoparticles form a labyrinthlike structure like in Fig. 5(b). After that, simple shears with a Péclet number of a range from 10 to 10^4 have been imposed. All simulations have been carried out until quasisteady structures of the nanoparticles are realized. It is decided that the quasisteady structures are realized when nondimensional boundary length, which is introduced in the next paragraph, becomes a plateau. Figure 7 shows snapshots of simulation results with different Péclet numbers where instantaneous streamlines are drawn by the line integral convolution (LIC) method [67,68]. The streamlines represent a flow field that is averaged over a time during which the solid walls move a distance of the diameter of a nanoparticle. When the Péclet number is 10 and 10^2, the colloidal

FIG. 8. Definition of boundary length of aggregated nanoparticles: bold black lines.

nanoparticles form a flawed crystalline structure throughout the domain. There are hexagonally close-packed nanoparticles in many areas of the domain. When the Péclet number is 10^3, on the other hand, there are few hexagonally close-packed nanoparticles and a network structure is formed. The structure of nanoparticles at Pe=10, 10^2, and 10^3 is well connected and does not change the whole shape with time. Therefore the solvent flows in a speed relative to the structure of nanoparticles. This argument is clearly shown by many vortices in voids of the structures. At the highest Péclet number of 10^4, there are less flawed and small crystals of the nanoparticles in the domain. The crystals are not well connected and the whole structure of nanoparticles changes its shape with time. In fact, the streamlines are almost parallel to the walls, and no vortex exists in the voids of the structure.

The self-organized structures of nanoparticles mentioned above are quantitatively evaluated by nondimensional boundary length (NBL) suggested by the authors. The NBL represents the ratio of boundary length of aggregated nanoparticles to the summation of boundary length of each nanoparticle. The definition of boundary length of aggregated nanoparticles is shown in Fig. 8. The NBL can be approximated using the coordinate number of each nanoparticle as

$$\mathrm{NBL} = \frac{1}{6N_p}\sum_{k=0}^{6}(6-n_c)N(n_c), \tag{50}$$

where $N(n_c)$ is the number of nanoparticles whose coordinate number is n_c. The NBL becomes 1 when all nanoparticles are completely dispersed. The NBL becomes 0 when all nanoparticles are hexagonally close packed. Namely, the NBL decreases as aggregation of the nanoparticles evolves. Figure 9 shows time history of NBL for different Péclet numbers. The NBL decreases with time and reaches a quasisteady state for every simulation. The NBLs of quasisteady states have almost the same value for Pe=10, 10^2, and 10^4, whereas the NBL for Pe=10^4 fluctuates considerably around the mean value. The fluctuation indicates the change of structure of nanoparticles with time. On the other hand, the NBL for Pe $=10^3$ is significantly larger than the NBLs for other Péclet numbers. The NBL for Pe=10^3 involves the network structure as shown in Fig. 7(c). There are incubation times for aggregation of the nanoparticles to occur for every simulation. The incubation times and the aggregation times decrease in inverse proportion to the Péclet number.

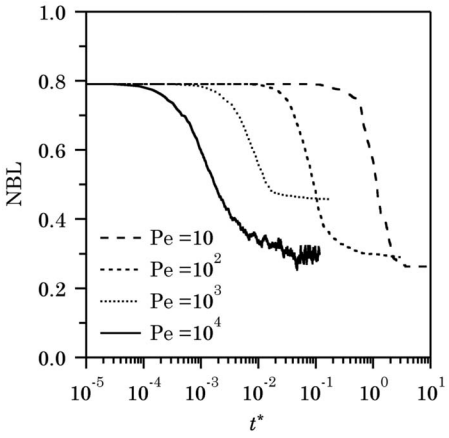

FIG. 9. Time history of NBL for different Péclet numbers.

Viscosity of a concentrated colloid depends strongly on self-organized structure of colloidal nanoparticles [69–71]. Apparent viscosity of the present colloidal nanoparticulate flows can be evaluated by the shear force that is exerted on the solid walls at the top and bottom boundaries. The specific apparent viscosity is obtained as

$$\frac{\eta_a}{\eta} = \frac{1}{\dot{\gamma}}\left(\frac{\partial \boldsymbol{u}}{\partial \boldsymbol{n}}\right)_w, \tag{51}$$

where η_a is the apparent viscosity and $(\partial \boldsymbol{u}/\partial \boldsymbol{n})_w$ is the velocity gradient in the direction normal to the wall. The velocity gradient is averaged over a time during which the quasisteady state is realized in Fig. 9. Figure 10 shows the variation of the specific apparent viscosity of the colloid with the Péclet number. The apparent viscosity of the colloid increases considerably over the viscosity of the solvent. The

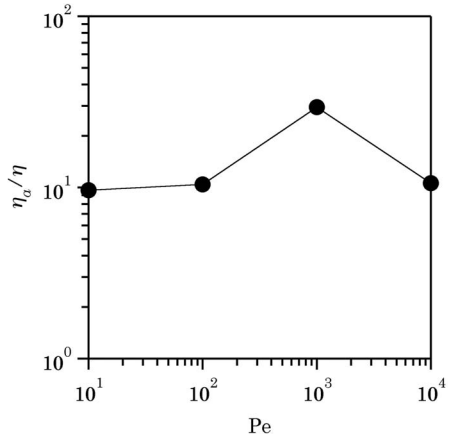

FIG. 10. Variation of specific apparent viscosity of colloid with Péclet number.

increment is much larger than the amount that is expected by the Einstein-Stokes law of viscosity, because the interaction between the nanoparticles is prominent for the concentrated colloid. The apparent viscosity has almost the same value for $\mathrm{Pe}=10$, 10^2, and 10^4. The fact relates directly to Figs. 7 and 9. Namely, the structure of the colloidal nanoparticles governs the viscosity of the colloid. The apparent viscosity for $\mathrm{Pe}=10^3$ is about three times larger than the apparent viscosity for other Péclet numbers. The fact implies that the network structure of nanoparticles in Fig. 7(c) leads to larger viscosity of the colloid than the crystalline structures of nanoparticles in Figs. 7(a), 7(b), and 7(d). The behavior of shear-thickening and shear-thinning shown in Fig. 10 agrees qualitatively with shear-induced gelation and shear yielding of a concentrated colloid in literature [72–75].

C. Computational efficiency

The computational efficiency of the present simulation model is argued here. Unlike the DLMFD method and the FPD method, the motion of particles and the flow of solvent can evolve with separate time steps in the present model. The ratio of both time steps $l_{\max}$ in Eq. (26) is 10 for every simulation in this paper, so that the computational cost to solve the hydrodynamic equation is reduced to a tithe of the computational cost of simulation using a common time step. In the simulation models that treat a liquid as an ensemble of particles, such as DPD, LB, and SRD, a time step by which the discretized model of liquid evolves is essentially restricted by a lattice spacing in a computational domain. In contrast, the simulation models where a liquid is treated by the fluctuating Navier-Stokes equation can employ an efficient implicit scheme. The present model allows a large time step for time evolution simulations by use of the SIMPLEST. For a low Reynolds number flow as is presented in this paper, the diffusion of liquid rather than the convection restricts the step of time evolution under the stability condition of the discretized equation. The stability condition in two dimensions relates to the diffusion number d as

$$d = \nu\left(\frac{1}{\Delta x^2} + \frac{1}{\Delta y^2}\right)\Delta t. \tag{52}$$

If a first-order explicit scheme is used to discretize the momentum equation, the stability condition is $d \leq 0.5$. On the other hand, d in the present simulations increases up to 6.3, that is, over 12 times larger than the above condition.

Furthermore, a fascinating novelty of the present simulation model is that the computational cost is constant regardless of the concentration of nanoparticles for a fixed computational domain. Figure 11 shows the variation of CPU time for each time step with the volume fraction of nanoparticles. The CPU time that is averaged over 1000 time steps is normalized by the value at the volume fraction of zero. As the volume fraction increases, the number of nanoparticles with which a nanoparticle interacts through the contact force and the DLVO force increases. Therefore the number of evaluations of the particle-to-particle interactions increases. Nevertheless, the CPU time for each time step does not increase although the volume fraction increases up to 0.5, as shown in Fig. 11. This can be due to a decrease of the amount of flow field computation that makes up the majority of total computation for each time step. Figure 12 shows the number of iterations that are required for the convergence of velocity field and pressure field for each time step. The number of iterations for the convergence of pressure field represents the maximum value for each time step. The number of iterations for the convergence of velocity field is constant regardless of the volume fraction since the convergence of velocity field depends mainly on Δt. On the other hand, the number of iterations for the convergence of pressure field decreases considerably as the volume fraction increases from 0.1 to 0.5. This is due to the pressure fix in the particle domain. The effect of pressure fix increases as the volume fraction, because the Poisson equation of pressure is not necessary to be solved in the particle domain. Consequently, the amount of flow field computation decreases as the volume fraction increases. The feature is very desirable for concentrated colloidal nanoparticulate flows.

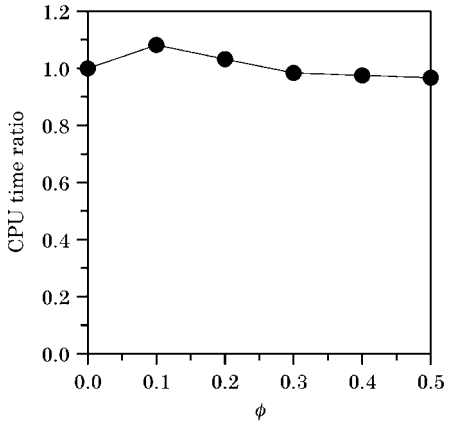

FIG. 11. Variation of CPU time for each time step with volume fraction of nanoparticles.

IV. CONCLUSIONS

The present simulation model includes contact interaction and DLVO interaction between the nanoparticles, and hydro-

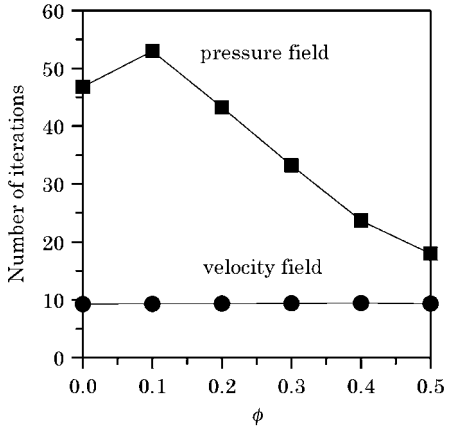

FIG. 12. Number of iterations for each time step required for convergence of velocity field and pressure field.

dynamic interaction between the nanoparticles and the solvent that satisfies the fluctuation-dissipation theorem. The model can be said to be an optimized combination of the above interactions for concentrated colloidal nanoparticulate flows. Compared to existing simulation models, the present model can have higher accuracy, robustness, and efficiency. The accuracy is obtained because the model includes all interactions required to calculate concentrated colloidal nanoparticulate flows. The robustness has been illustrated by the simulations of aggregated systems that may lead to numerical instabilities when the existing simulation model is adopted. The efficiency is obtained by the fictitious domain (FD) method to couple the motion of nanoparticles with the flow of the solvent, the dual time stepping for time evolution, the pressure fix in the particle domain, and second-order SIMPLEST to solve the hydrodynamic equation. In fact, the computational effort for concentrated systems by the present model is almost the same as the computational effort for single-phase systems without particles. This is a fascinating novelty of the present simulation model. The computational cost of the present model can be additionally reduced if a multigrid method is adopted to solve the Poisson equation of pressure. The present model is applicable to complicated geometries since the boundary condition of solid wall can be easily imposed on any lattice point through the volume fraction of a solid with zero velocity. Simulation results have shown that the present model has a capability to reproduce self-organizations of concentrated colloidal nanoparticles in shear flows and reveal the relationship between the self-organized structure of nanoparticles and the viscosity of a colloid. A typical time evolution simulation has taken less than a day on a high performance personal computer with four CPUs. Although the simulation results in this paper are limited to two dimensions, extension of the model to three dimensions is straightforward. A three-dimensional simulation of concentrated colloidal nanoparticulate flow by the present model will be presented in the near future. The authors expect that the present simulation model will become a powerful tool to elucidate the mechanism of self-organization of concentrated colloidal nanoparticles in a flow.

[1] B. T. Holland, C. F. Blanford, and A. Stein, Science **281**, 538 (1998).
[2] J. E. G. J. Wijnhoven and W. L. Vos, Science **281**, 802 (1998).
[3] M. P. Pileni, J. Phys. Chem. B **105**, 3358 (2001).
[4] M. K. Corbierre, N. S. Cameron, M. Sutton, S. G. J. Mochrie, L. B. Lurio, A. Rühm, and R. B. Lennox, J. Am. Chem. Soc. **123**, 10411 (2001).
[5] T. Okubo, S. Chujo, S. Maenosono, and Y. Yamaguchi, J. Nanoparticle Res. **5**, 111 (2003).
[6] I. Hussain, M. Brust, A. J. Papworth, and A. I. Cooper, Langmuir **19**, 4831 (2003).
[7] Z. H. Mbhele, M. G. Salemane, C. G. C. E. van Sittert, J. M. Nadeljković, V. Djoković, and A. S. Luyt, Chem. Mater. **15**, 5019 (2003).
[8] F. Juillerat, P. Bowen, and H. Hofmann, Langmuir **22**, 2249 (2006).
[9] D. L. Ermak and J. A. McCammon, J. Chem. Phys. **69**, 1352 (1978).
[10] S. R. Rastogi and N. J. Wagner, Comput. Chem. Eng. **19**, 693 (1995).
[11] T. N. Phung, J. F. Brady, and G. Bossis, J. Fluid Mech. **313**, 181 (1996).
[12] A. Sierou and J. F. Brady, J. Fluid Mech. **448**, 115 (2001).
[13] M. Das, S. Ramaswamy, A. K. Sood, and G. Ananthakrishna, Phys. Rev. E **73**, 061409 (2006).
[14] P. J. Hoogerbrugge and J. M. V. A. Koelman, Europhys. Lett. **19**, 155 (1992).
[15] E. S. Boek, P. V. Coveney, H. N. W. Lekkerkerker, and P. van der Schoot, Phys. Rev. E **55**, 3124 (1997).
[16] S. Haber, N. Filipovic, M. Kojic, and A. Tsuda, Phys. Rev. E **74**, 046701 (2006).
[17] A. Tiwari and J. Abraham, Phys. Rev. E **74**, 056701 (2006).
[18] L. D. Landau and E. M. Lifshitz, *Fluid Mechanics* (Pergamon Press, London, 1959).
[19] R. F. Fox and G. E. Uhlenbeck, Phys. Fluids **13**, 1893 (1970).
[20] G. Khujadze, M. Oberlack, and G. Chagelishvili, Phys. Rev. Lett. **97**, 034501 (2006).
[21] N. Sharma and N. A. Patankar, J. Comput. Phys. **201**, 466 (2004).
[22] P. Atzberger, Phys. Lett. A **351**, 225 (2006).
[23] C. S. Peskin, Acta Numerica **11**, 479 (2002).
[24] M. Uhlmann, J. Comput. Phys. **209**, 448 (2005).
[25] D. Kim and H. Choi, J. Comput. Phys. **212**, 662 (2006).
[26] R. Glowinski, T.-W. Pan, T. I. Hesla, and D. D. Joseph, Int. J. Multiphase Flow **25**, 755 (1999).
[27] N. Sharma and A. Patankar, J. Comput. Phys. **205**, 439 (2005).
[28] Z. Yu, X. Shao, and A. Wachs, J. Comput. Phys. **217**, 424 (2006).
[29] H. Tanaka and T. Araki, Phys. Rev. Lett. **85**, 1338 (2000).
[30] A. J. C. Ladd, Phys. Rev. Lett. **70**, 1339 (1993).
[31] A. J. C. Ladd, J. Fluid Mech. **271**, 285 (1994).
[32] A. J. C. Ladd, J. Fluid Mech. **271**, 311 (1994).
[33] O. Behrend, Phys. Rev. E **52**, 1164 (1995).
[34] P. N. Segrè, O. P. Behrend, and P. N. Pusey, Phys. Rev. E **52**, 5070 (1995).
[35] O. Berk Usta, A. J. C. Ladd, and J. E. Butler, J. Chem. Phys. **122**, 094902 (2005).
[36] R. Adhikari, K. Stratford, M. E. Cates, and A. J. Wagner, Europhys. Lett. **71**, 473 (2005).
[37] G. R. McNamara and G. Zanetti, Phys. Rev. Lett. **61**, 2332 (1988).
[38] S. Chen, Z. Wang, X. Shan, and G. D. Doolen, J. Stat. Phys. **68**, 379 (1992).
[39] A. Malevanets and R. Kapral, J. Chem. Phys. **110**, 8605 (1999).
[40] A. Malevanets and R. Kapral, J. Chem. Phys. **112**, 7260 (2000).
[41] G. A. Bird, Comput. Math. Appl. **35**, 1 (1998).

[42] M. Hecht, J. Harting, M. Bier, J. Reinshagen, and H. J. Herrmann, Phys. Rev. E **74**, 021403 (2006).
[43] J. T. Padding and A. A. Louis, Phys. Rev. E **74**, 031402 (2006).
[44] J. N. Israelachvili, *Intermolecular and Surface Forces* (Academic Press, London, 1992).
[45] P. A. Cundall and O. D. L. Strack, Geotechnique **29**, 47 (1979).
[46] Y. Tsuji, T. Tanaka, and T. Ishida, Powder Technol. **71**, 239 (1992).
[47] L. Popken and P. W. Cleary, J. Comput. Phys. **155**, 1 (1999).
[48] D. B. Spalding, Math. Comput. Simul. **23**, 267 (1981).
[49] S. V. Patankar and D. B. Spalding, Int. J. Heat Mass Transfer **15**, 1787 (1972).
[50] M. Fujita and Y. Yamaguchi, J. Comput. Phys. **223**, 108 (2007).
[51] C. W. Hirt and J. L. Cook, J. Comput. Phys. **10**, 324 (1972).
[52] W. Kalthoff, S. Schwarzer, and H. J. Herrmann, Phys. Rev. E **56**, 2234 (1997).
[53] K. Höfler and S. Schwarzer, Phys. Rev. E **61**, 7146 (2000).
[54] S. P. Timoshenko and J. N. Goodier, *Theory of Elasticity* (McGraw-Hill, New York, 1970).
[55] R. D. Mindlin and H. Deresiewicz, J. Appl. Mech. **20**, 327 (1953).
[56] S. Wall, W. John, H. C. Wang, and S. L. Goren, Aerosol Sci. Technol. **12**, 926 (1990).
[57] S. F. Foerster, M. Y. Louge, H. Chang, and K. Allia, Phys. Fluids **6**, 1108 (1994).
[58] R. Ramírez, T. Pöschel, N. V. Brilliantov, and T. Schwager, Phys. Rev. E **60**, 4465 (1999).
[59] T. Schwager, Phys. Rev. E **75**, 051305 (2007).
[60] R. Yamamoto, Y. Nakayama, and K. Kim, J. Phys.: Condens. Matter **16**, S1945 (2004).
[61] S. Yamamoto and T. Matsuoka, J. Chem. Phys. **107**, 3300 (1997).
[62] A. J. C. Ladd and R. Verberg, J. Stat. Phys. **104**, 1191 (2001).
[63] J. Kromkamp, D. T. M. van den Ende, D. Kandhai, R. G. M. van der Sman, and R. M. Boom, J. Fluid Mech. **529**, 253 (2005).
[64] J. R. Fox and H. C. Andersen, J. Phys. Chem. **88**, 4019 (1984).
[65] W. Hackbusch, *Multi-Grid Methods and Applications* (Springer-Verlag, Berlin, 1985).
[66] R. E. Ewing, BIT **29**, 850 (1989).
[67] B. Cabral and L. Leedom, *Computer Graphics Proceedings* (ACM SIGGRAPH, Anaheim, 1993), p. 263.
[68] L. K. Forssell and S. D. Cohen, IEEE Trans. Vis. Comput. Graph. **1**, 133 (1995).
[69] D. R. Foss and J. F. Brady, J. Fluid Mech. **407**, 167 (2000).
[70] W. J. Tseng and K.-C. Lin, Mater. Sci. Eng., A **355**, 186 (2003).
[71] J. Vermant and M. J. Solomon, J. Phys.: Condens. Matter **17**, R187 (2005).
[72] R. Wessel and R. C. Ball, Phys. Rev. A **46**, R3008 (1992).
[73] G. Petekidis, P. N. Pusey, A. Moussaïd, S. Egelhaaf, and W. C. K. Poon, Physica A **306**, 334 (2002).
[74] M. L. Kilfoil, E. E. Pashkovski, J. A. Masters, and D. A. Weitz, Philos. Trans. R. Soc. London, Ser. A **361**, 753 (2003).
[75] D. Lootens, P. Hébraud, E. Lécolier, and H. Van Damme, Oil Gas Sci. Technol. **59**, 31 (2004).